

ARMY RESEARCH LABORATORY



Flat Fire Jump Performance of a 155-mm M198 Howitzer

James M. Garner
Bernard J. Guidos
Keith P. Soencksen
David W. Webb

ARL-TR-2067

SEPTEMBER 1999

19991026 122

Approved for public release; distribution is unlimited.

The findings in this report are not to be construed as an official Department of the Army position unless so designated by other authorized documents.

Citation of manufacturer's or trade names does not constitute an official endorsement or approval of the use thereof.

Destroy this report when it is no longer needed. Do not return it to the originator.

Army Research Laboratory

Aberdeen Proving Ground, MD 21005-5066

ARL-TR-2067

September 1999

Flat Fire Jump Performance of a 155-mm M198 Howitzer

James M. Garner
Bernard J. Guidos
Keith P. Soencksen
David W. Webb
Weapons & Materials Research Directorate

Approved for public release; distribution is unlimited.

Abstract

A jump experiment and analysis were performed for the M198 howitzer firing the M107 shell through short range, flat fire trajectories with a launch Mach number near 1.7. The objective was to characterize the jump performance of the system and provide a basis for identifying and possibly improving the largest contributors to jump over a broader range of firing conditions. For the short range, flat fire scenario of the present experiment, the jump performance of the system indicates that the center of gravity (CG) motion of the projectile as it exits the gun tube is a significantly larger contributor to dispersion than the aerodynamic jump. The data showed that the projectile CG motion relative to the muzzle itself is considerable and is a more dominant component of in-bore balloting in terms of dispersion compared to the in-bore angular motion. Measurements of the gun dynamics showed that while the large scale muzzle motion is more pronounced in the vertical plane than in the horizontal plane, the dispersion directly attributable to muzzle pointing angle and muzzle crossing velocity is about the same in the both directions. Measurements of muzzle velocity, drag, and yaw are also presented and can be used to determine the effect of jump components not directly measured here but important for longer ranges.

TABLE OF CONTENTS

	<u>Page</u>
LIST OF FIGURES	v
LIST OF TABLES	vii
1. INTRODUCTION	1
2. SETUP	2
2.1 Instrumentation	2
3. DEFINITIONS OF JUMP COMPONENTS	4
4. RESULTS	8
4.1 Total Jump	9
4.2 Muzzle Motion	10
4.3 Aerodynamics	13
4.4 CG Motion at Muzzle	18
4.5 Correlations Between Jump Components	20
5. CONCLUSION	25
REFERENCES	29
APPENDICES	
A. M107 Jump Statistical Review	31
B. List of Symbols	35
DISTRIBUTION LIST	39
REPORT DOCUMENTATION PAGE	41

INTENTIONALLY LEFT BLANK

LIST OF FIGURES

<u>Figure</u>		<u>Page</u>
1.	Diagnostic Schematic for the M198 Jump Experiment	2
2.	Spade Stop Configuration	3
3.	Illustration of Jump Angles	5
4.	Jump Closure Model	5
5.	Total Jump for All Shots	9
6.	Tube Center Line Vertical Displacement at 38.7 cm From Muzzle, Shot 34540 . .	11
7.	Tube Center Line Horizontal Displacement at 38.7 cm From Muzzle, Shot 34540	12
8.	Vertical Component of Muzzle Pointing Angle Versus Time, Shot 34540	12
9.	Horizontal Component of Muzzle Pointing Angle Versus Time, Shot 34540	13
10.	Muzzle Pointing Angle at Shot Exit	14
11.	Muzzle Crossing Velocity (CV) Jump	14
12.	Initial Pitch and Yaw Angles	16
13.	Spin Contribution to Aerodynamic Jump	16
14.	Initial Angular Rates in Pitch and Yaw	17
15.	Aerodynamic Jump	18
16.	CG Jump	19
17.	Total CG Jump	19
18.	Matrix Plot for Total Jump and All Jump Components, Azimuth	22
19.	Matrix Plot for Total Jump and All Jump Components, Elevation	22
20.	Matrix Plot for Total Jump, CG_{TOT} , and AJ Jump Components, Azimuth	24
21.	Matrix Plot for Total Jump, CG_{TOT} , and AJ Jump Components, Elevation	25
22.	M107 Jump Closure	26

INTENTIONALLY LEFT BLANK

LIST OF TABLES

<u>Table</u>		<u>Page</u>
1.	Measured Jump and Components	8
2.	Group Mean and Dispersion of Jump Components	9
3.	Other Measured Jump Components of Interest	10
4.	Group Means and Dispersions for Other Jump Components of Interest	10
5.	Drag and Mean Squared Yaw	15
6.	Correlation Matrices for Total Jump and All Jump Components	21
7.	Correlation Matrices for Total Jump, CG_{TOT} , and AJ Jump Components	24

INTENTIONALLY LEFT BLANK

FLAT FIRE JUMP PERFORMANCE OF A 155-MM M198 HOWITZER

1. INTRODUCTION

Large caliber artillery systems are often classed as "area" weapons whose targets are robust at long range and dispersed. Under these conditions, the effectiveness of some systems depends upon the ability to have a forward observer (FO) communicate the first round impact location, allowing the gun crew to correct and fire again. Not only does this reduce the element of surprise, but having an FO in a potentially hostile area is distinctly problematic. The capability of artillery systems to fire initially for effect rather than calibration is generating more interest as the benefits of first round accuracy are being recognized. A fundamental understanding of the processes that affect artillery accuracy and precision is needed to identify the largest sources of error in the system. The projectile and muzzle conditions at shot exit can be measured and related to accuracy and precision, thereby leading to focused efforts for system improvement.

The Aerodynamics Branch of the Weapons and Materials Research Directorate of the U.S. Army Research Laboratory (ARL), sponsored by the Advanced Weapons Concepts Branch, ARL, conducted an experiment at the Transonic Experimental Facility (TEF), Aberdeen Proving Ground, Maryland (Rogers 1969) to examine the jump characteristics of an M198 howitzer system. This system was chosen because it is widely used and because future 155-mm systems will likely be judged by their performance in comparison to it. Additionally, it has been suggested that a single caliber for all artillery would have substantial logistical and economic benefits, and the caliber of choice by many indicators is 155 mm.

ARL has demonstrated success in characterizing large caliber tank gun accuracy and performance through jump measurements (Bornstein, Celmins, Plostins & Schmidt 1988). The jump vectors represent the dominant lateral disturbances to which the round is subjected during launch and flight. This report describes the results of a jump experiment and analysis of M107 projectiles fired from an M198 howitzer. The analysis and terminology used to characterize the jump of direct fire weapons are adapted here to describe the jump of an indirect fire artillery system. This experiment represents an initial effort focusing on low elevation firings (i.e., flat fire trajectories) and will contribute to a larger database that characterizes the weapon system performance over a range of firing conditions.

2. SETUP

2.1 Instrumentation

An M198 system, breech ring serial number (S/N) 334, was provided by ARL for use at TEF. The gun tube, S/N 29094, was considered to be of low wear, rated at 94% life. The diagnostic setup consisted of eight proximity probes placed near the muzzle, four orthogonal X-ray stations positioned from muzzle exit to 8 m range, and 25 orthogonal spark shadowgraph stations spaced roughly from 30 m to 240 m range. A cloth target was placed at 298 m range to measure target impacts and dispersion. While a greater target distance was desired, the inclement weather and strong winds dictated that the target be placed inside the spark shadowgraph facility. Additionally, high speed cameras were placed in front of the entrance at about 12 m from the muzzle.

Figure 1 shows a schematic of the instrumentation setup. The proximity probes record muzzle motion during the launch cycle, providing as output the muzzle pointing angle and crossing velocity at shot exit. The X-ray images record the projectile location and orientation near the muzzle, in lieu of standard photographs that can be obscured by smoke and flash from the launch event. The 25 shadowgraph stations determine the projectile location and orientation at selected locations within the building.

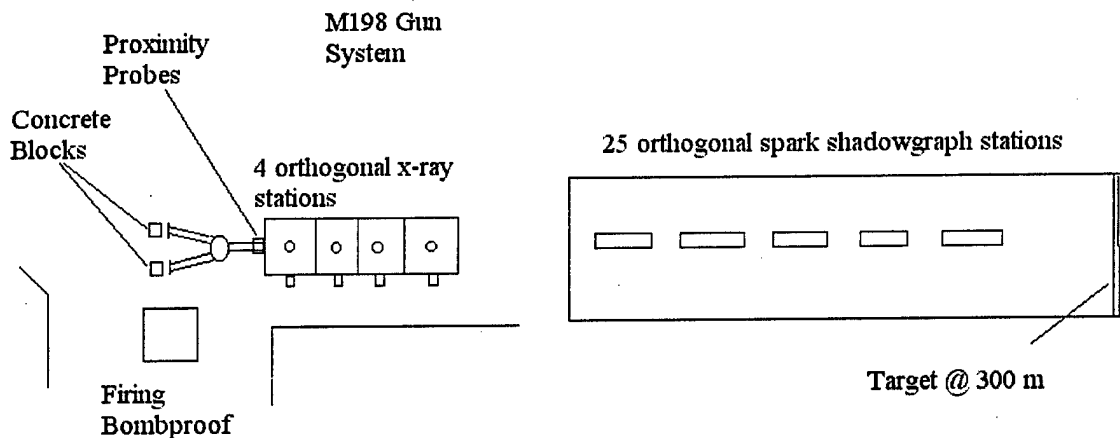


Figure 1. Diagnostic Schematic for the M198 Jump Experiment.

A setup detail of particular interest is the method of securing the artillery mount to the ground. Large caliber artillery mounts have spades that prevent excessive mount motion during firing. However, the gun system was positioned on an asphalt surface adjacent to the entrance of the spark shadowgraph facility, and excavating the asphalt to accommodate the spades was an

undesirable option. Because the recoil of the gun system is affected by how the system's spades are placed, a realistic solution was needed. The solution chosen here was to wedge each spade against a pile of sand bags backed with a stack of concrete blocks, as shown in Figure 2. The mass of each of the two concrete stacks was estimated to be 5340 kg. Polyester straps (not shown in the figure) were attached to lifting "eyes" on the howitzer and to other lifting eyes welded to plates on the ground. This restricted the gun system from pivoting about the spades and from interfering with the re-initialization of the instrumentation for subsequent shots. The straps allowed some motion of the system, particularly during the first shot, but adequately limited excessive motion overall.

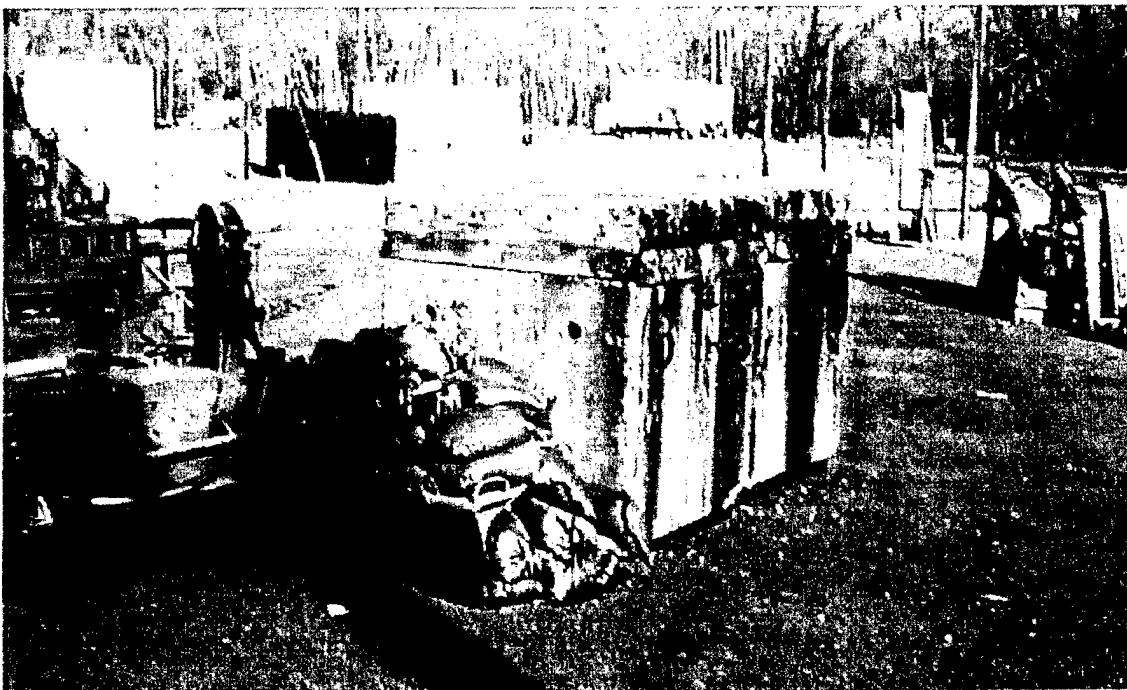


Figure 2. Spade Stop Configuration.

The M4A2 Zone 7 (7W) propelling charge was selected in consideration of future lightweight howitzer systems operations. This charge produces a nominal projectile muzzle velocity of 568 m/s (Department of the Army 1969). The rounds were fired at an elevation of 10 milliradians (mrad), allowing the fired projectiles to enter and exit the spark shadowgraph facility without damaging instrumentation.

3. DEFINITIONS OF JUMP COMPONENTS

The data acquired for each shot provide a variety of information concerning the launch and flight behavior of the rounds. A substantial portion of the data is then used to construct a jump diagram for each shot. The jump diagrams are based upon a jump closure model that characterizes the launch and flight aspects of a projectile, in addition to providing a basis for statistical analysis of the entire set of rounds. The jump model has been presented along with the analysis techniques in reports by Bornstein et al. (1988, 1989) and Plostins, Celmins, and Bornstein (1990) and is briefly reviewed here.

The total jump of a particular shot is defined using the nomenclature introduced in Figure 3. The boresight line of fire (LOF) is established as the line connecting the center of the muzzle and the visual aim point (boresight point). The gravity drop can be extracted separately from various data sources, including the radar track, and is considered known. The LOF combined with the known gravity drop establishes a target aim point from which the target impact point is measured. The resulting vector is denoted as (X_T, Y_T) , with the subscript T representing the values at the target impact point. For the present conditions, the magnitude of this vector is small enough compared to the target range R_T that the vector may be converted directly into an angle forming the total jump angle (or simply "jump"), denoted θ , i.e.,

$$\theta = \theta_h \mathbf{i} + \theta_v \mathbf{j} \cong X_T / R_T \mathbf{i} + Y_T / R_T \mathbf{j} \quad \text{Eq (1)}$$

in which θ_h and θ_v are the horizontal and vertical components, respectively, of the total jump. The unit vector \mathbf{i} is oriented to the gunner's right (positive X in Figure 3) and denotes positive azimuth (AZ). The unit vector \mathbf{j} is oriented up (positive Y in Figure 3) and represents positive elevation (EL). These vector orientations represent jump coordinates as used in this report.

The jump closure model is shown in Figure 4. The origin is defined as the intersection of the horizontal and vertical axes (labeled H and V) and represents the aim point. The target impact point is denoted as a solid circle. A set of vectors is defined whose summation is equal to the total jump vector, the vector whose tail is located at the aim point and whose head is located at the target impact point. These vectors are jump component vectors, each having a horizontal and vertical component. For the spinning artillery shell and flat fire scenario, the relevant jump vectors are defined as follows, with additional discussion following:

1. Muzzle Pointing Angle (PA) Jump - The angular deviation of the projectile corresponding to the muzzle pointing angle at the time of shot exit relative to boresight LOF.

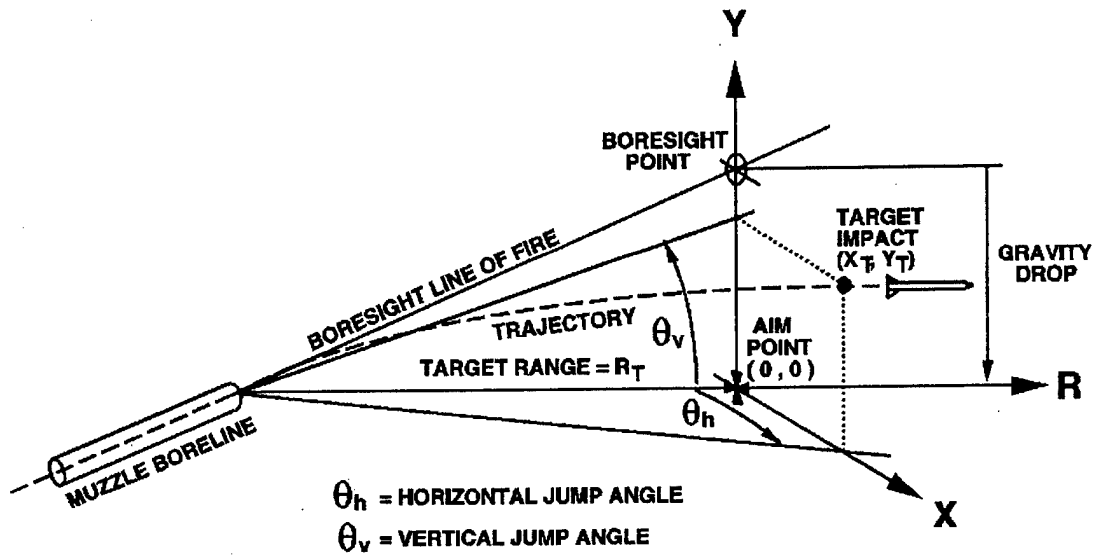


Figure 3. Illustration of Jump Angles.

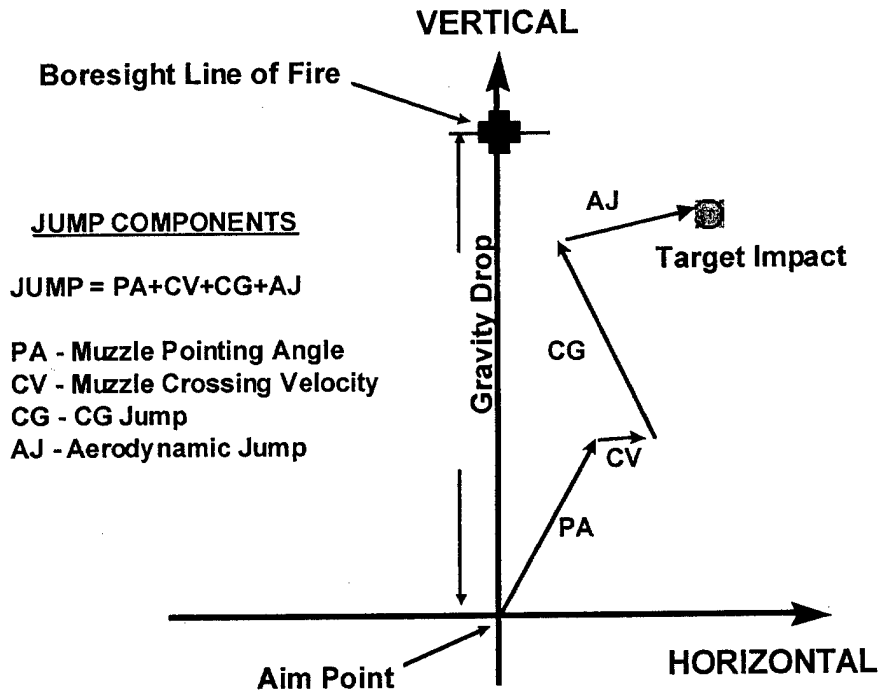


Figure 4. Jump Closure Model.

2. Muzzle Crossing Velocity (CV) Jump - The angular deviation of the projectile corresponding to the muzzle lateral motion, obtained by dividing the muzzle lateral velocity at shot exit by the projectile launch velocity.

3. CG Jump - The angular deviation of the projectile at the muzzle relative to the instantaneous muzzle center line at shot exit. Also referred to in previous jump experiments as the jump attributable to mechanical disengagement of the projectile from the gun tube, CG jump is measured relative to a coordinate system attached to the muzzle.

4. Aerodynamic Jump (AJ) - The angular deviation of the projectile attributable to aerodynamic lift forces associated with projectile yawing motion.

The PA and CV jump components are obtained by reducing eddy probe data as outlined by Bornstein et al. (1988). The values are extracted from the data at a time that corresponds to shot exit, defined here as the instant in time when the projectile rotating band mechanically disengages from the gun tube and the main blast uncorks.

The aerodynamic jump for each shot is calculated using motion parameters obtained from a least squares fit of the spark shadowgraph facility data and X-ray data to the linearized free flight equations of angular motion for a spinning projectile (Murphy 1963). The aerodynamic jump, J_A , is calculated using aerodynamic coordinates and complex notation consistent with Murphy. McCoy (1998) has derived the additional spin contribution to aerodynamic jump, and using Murphy's notation, the expression is rewritten as

$$J_A = k_t^2 C_{L\alpha} / C_{M\alpha} (\xi_o' - iP\xi_o) \quad \text{Eq (2)}$$

In this expression, k_t is the sub-projectile transverse radius of gyration, $C_{M\alpha}$ is the sub-projectile pitching moment coefficient, $C_{L\alpha}$ is the projectile lift coefficient, and P is a scaled spin rate. ξ_o and ξ_o' are the initial sub-projectile complex yaw angle (radians) and transverse angular rate (in radians/caliber of travel), respectively, evaluated at the muzzle.

The projectile angle of attack, ξ , is defined here to be consistent with Murphy (1963), i.e.,

$$\xi = \beta + i\alpha \quad \text{Eq (3)}$$

in which α is the pitch angle (positive nose up) and β is the yaw angle (positive nose to the gunner's left).

The conversion of the aerodynamic jump from aerodynamic coordinates to jump coordinates is

$$AJ = \text{Re}(J_A)i - \text{Im}(J_A)j \quad \text{Eq (4)}$$

The transformation recognizes that the sign of the vertical displacement in jump coordinates is positive up but is positive down in Murphy's aerodynamic coordinates.

The CG jump is predominantly a measure of the projectile's in-bore CG motion relative to the instantaneous lateral muzzle motion at shot exit. After the impact point, gravity drop, PA, CV, and AJ jump components are determined, the CG jump is obtained by applying closure to the system. This also allows a separate jump component, the total CG jump, or CG_{TOT} , to be defined as the sum of the PA, CV, and CG jump vectors. CG_{TOT} represents the total lateral CG motion at shot exit relative to the boresight LOF. The standard deviation (SD) of error of the measurement system is estimated to be on the order of 0.2 mrad. This is about the same as that estimated by Lyon, Savick, and Schmidt (1991).

Alternatively, the CG jump can be determined from direct measurement of the CG motion in the X-ray photographs but with less accuracy. In that approach, the projectile CG is measured in the X-ray photographs relative to the fiducial beads. These CGs are then numerically fitted using a least squares procedure to determine CG_{TOT} . The CG jump can then be determined by subtracting PA and CV from CG_{TOT} . The estimated SD of the error in CG_{TOT} using this method is 0.35 mrad. Measurement of the CGs from the X-ray photographs was performed here as a standard procedure, but a review of the CG data showed that station-to-station variations for some shots were unrealistically large. Following these considerations, closure is the chosen method used here to determine the CG_{TOT} and CG jump vectors.

The epicyclic component of the total swerve is a fluctuating aerodynamic lift effect that normally becomes insignificant at longer ranges for a stable, adequately damped projectile. At the relatively short target range of 298 m in the present study, the contribution can be significant for certain projectiles and conditions. The expression given by McCoy (1998) for calculating the helical radius that represents the epicyclic swerve for a gyroscopically stable projectile was used with the fitted flight parameters of the shots in this study. Although two shots had contributions on the order of 0.1 mrad, most had contributions on the order of 0.05 mrad. These are comparatively small magnitudes, and so the epicyclic contributions to swerve were assumed to be small enough to be absorbed into the aerodynamic jump and were not considered as a separate jump component.

Several other contributors to total jump, while not included in the jump model of this study, merit discussion. Typical of most artillery, the M107 projectile does not have a sabot, and therefore, jump attributable to sabot discard is nonexistent for this system. Also, any jump disturbance attributable to muzzle blast is assumed to be negligible. The drift of a spinning shell, as given by McCoy (1998), was also found to be negligible for the short target range of the

present study. The effect of drag variations on the jump of individual rounds is negligible for the short target range used here, although long range dispersion would require such consideration. Variations in muzzle velocity can also contribute to dispersion at long ranges, as can meteorological considerations, including wind.

4. RESULTS

A total of 11 rounds, Shots 34537 through 34547, was fired, as shown in Table 1, with complete jump data obtained for eight of the rounds. The three rounds with incomplete data were Shot 34537, in which one eddy probe signal was not obtained; Shot 34544, in which no X-ray images were obtained at Stations 3 and 4; and Shot 34545, in which one eddy probe signal was lost around shot exit. The incomplete data from these three shots are presented and labeled as such. X-ray images at one station were unavailable for Shots 34541 and 34542, but the data from the remaining three stations were used in the analysis, and these two shots are considered to have complete data.

Table 1. Measured Jump and Components

Shot	PA		CV		CG		AJ		Total	
	AZ	EL	AZ	EL	AZ	EL	AZ	EL	AZ	EL
34537	NA	NA	NA	NA	NA	NA	0.13	-0.10	0.76	0.59
34538	-0.95	1.29	0.12	-1.05	0.50	0.62	0.02	0.14	-0.31	1.00
34539	-0.60	1.37	-0.13	-0.80	0.80	0.96	0.02	0.11	0.09	1.61
34540	-0.71	1.46	-0.53	-1.00	2.18	1.14	-0.24	0.04	0.69	1.65
34541	-0.61	1.45	-0.49	-0.64	2.55	0.19	-0.27	-0.14	1.19	0.86
34542	-0.77	1.33	-0.86	-0.84	2.85	0.28	-0.03	0.03	1.19	0.81
34543	-0.60	1.09	-0.37	-0.91	1.30	0.85	0.04	0.27	0.38	1.30
34544	NA	NA	NA	NA	NA	NA	NA	NA	0.93	0.90
34545	NA	NA	NA	NA	NA	NA	-0.11	0.09	-0.42	1.03
34546	-0.61	1.50	-0.69	-1.86	1.89	1.93	0.10	-0.06	0.69	1.51
34547	-0.58	1.24	-0.32	-0.64	1.22	0.45	-0.13	-0.03	0.19	1.03

Note: All units are expressed in mrad

4.1 Total Jump

The total jump for all rounds is shown in Figure 5. The total jump represents the target impact locations without the gravity drop. The gravity drop is taken to be the same for all shots, calculated to be 1.45 meters at 298 m range, or 4.86 mrad. The total jump and jump components are tabulated in Table 1. The mean and the SDs of dispersion of the jump and jump components are tabulated in Table 2 and exclude the three shots with incomplete data. The mean impact locations and SDs of dispersion are calculated by considering the impacts in azimuth and elevation separately, i.e., directionally de-coupled. Appendix A shows graphic comparisons of these tabulated values. As a reminder, positive azimuth is to the gunner's right and positive elevation is up.

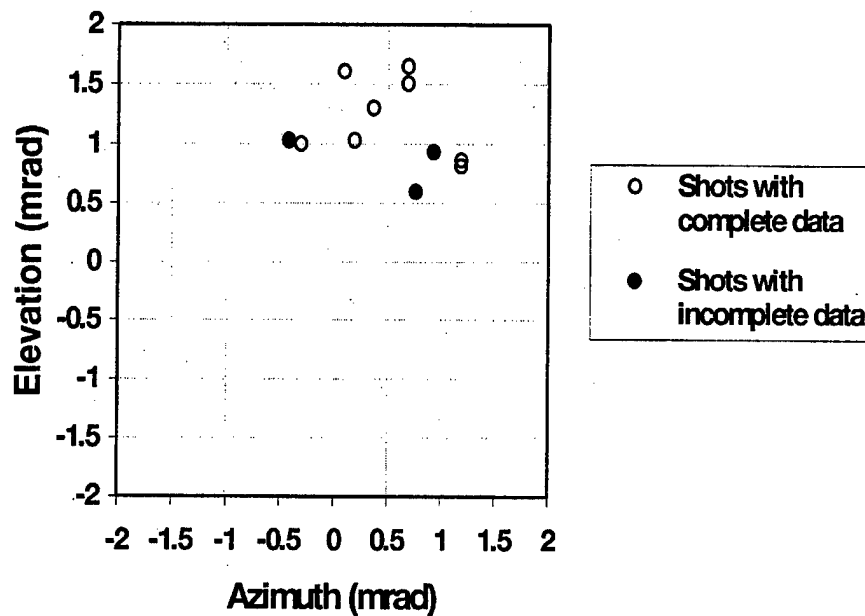


Figure 5. Total Jump for All Shots.

Table 2. Group Mean and Dispersion of Jump Components

Jump Components	Mean		Dispersion	
	AZ	EL	AZ	EL
PA	-0.679	1.342	0.128	0.136
CV	-0.411	-0.971	0.309	0.389
CG	1.662	0.803	0.840	0.562
AJ	-0.061	0.044	0.138	0.130
Total Jump	0.511	1.218	0.527	0.339

Note: All units are expressed in mrad

The group mean impact location is approximately 0.51 mrad right and 1.22 mrad up. The SD of the group dispersion is 0.53 mrad in azimuth and 0.34 mrad in elevation. The complete set of measured jump components is presented and discussed throughout the remainder of the section. Tables 3 and 4 contain other jump vectors of interest to be presented and discussed.

Table 3. Other Measured Jump Components of Interest

Shot	CG _{TOT}		AJ _S	
	AZ	EL	AZ	EL
34537	0.64	0.69	0.00	0.00
34538	-0.33	0.85	0.07	-0.01
34539	0.07	1.50	0.10	-0.04
34540	0.93	1.61	0.00	-0.15
34541	1.46	1.00	0.09	-0.13
34542	1.22	0.78	0.00	0.00
34543	0.33	1.03	0.34	0.08
34544	NA	NA	NA	NA
34545	0.31	0.93	0.08	0.04
34546	0.58	1.57	-0.02	-0.08
34547	0.32	1.06	0.08	-0.02

Note: All units are expressed in mrad

Table 4. Group Means and Dispersions for Other Jump Components of Interest

Jump Component	Mean		Dispersion	
	AZ	EL	AZ	EL
CG _{TOT}	0.572	1.174	0.600	0.332
AJ _S	0.083	0.043	0.114	0.074

Note: All units are expressed in mrad

4.2 Muzzle Motion

Eddy probe data were collected and reduced using the approach described by Bornstein and Haug (1988). The eddy probes were mounted near the gun tube surface at two stations approximately 38.7 cm (15.2 in) and 53.9 cm (21.2 in) from the muzzle. Examples of the reduced

data showing typical gun tube center line lateral motion histories at the station nearer to the muzzle are shown in Figures 6 and 7 for Shot 34540. The time is referenced to the pressure probe trigger with shot exit occurring at approximately -1.36 ms. This difference between shot exit time and probe trigger time is called the trigger delay time and is found for each shot by extrapolating the delay times of the X-ray images of the projectile up range to where mechanical disengagement occurs. The total in-bore time is approximately 20 ms, although the plots do not show the entire in-bore event. The large scale motion of the center line is down and to the left near the time of shot exit. This motion is more pronounced in the vertical plane than in the horizontal plane. During the in-bore time interval shown in the figures, the maximum vertical center line motion (approximately 0.6 mm in magnitude) is greater than the maximum horizontal motion (approximately 0.2 mm in magnitude). The same observation is also true for the displacements near shot exit.

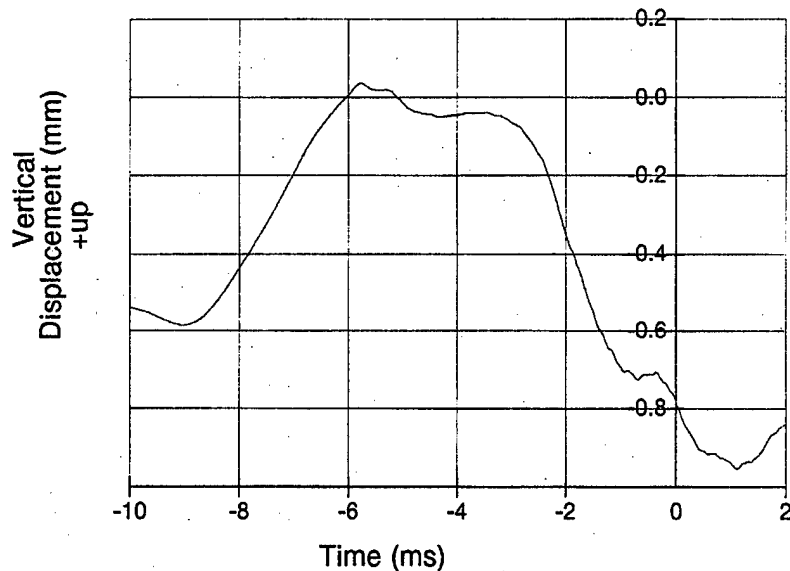


Figure 6. Tube Center Line Vertical Displacement at 38.7 cm From Muzzle, Shot 34540.

The displacement data from the two axial stations are combined to give the muzzle pointing angle. The angle calculated at the probe stations is assumed to be equal to the angle at the muzzle itself. Figures 8 and 9 show the vertical and horizontal muzzle pointing angle histories, respectively, for Shot 34540. The muzzle pointing angle, like the center line displacements, shows more pronounced motion in the vertical plane than in the horizontal plane. During the in-bore time interval shown in the figures, the maximum vertical pointing angle (approximately 1.7 mrad in magnitude) is greater than maximum horizontal pointing angle (approximately 0.7 mrad in

magnitude). The pointing angles in both directions show the presence of small scale oscillatory motions not apparent in the center line displacement plots. The behavior of the pointing angle plots was typical for all shots.

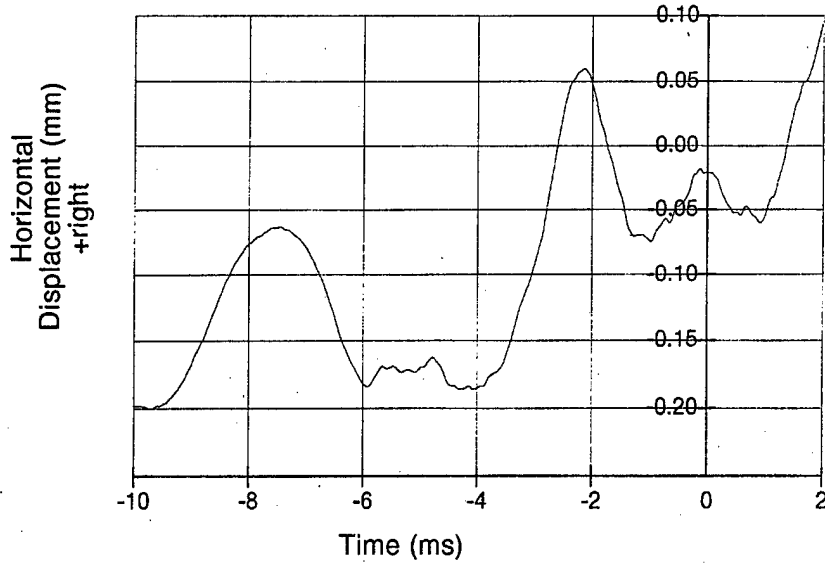


Figure 7. Tube Center Line Horizontal Displacement at 38.7 cm From Muzzle, Shot 34540.

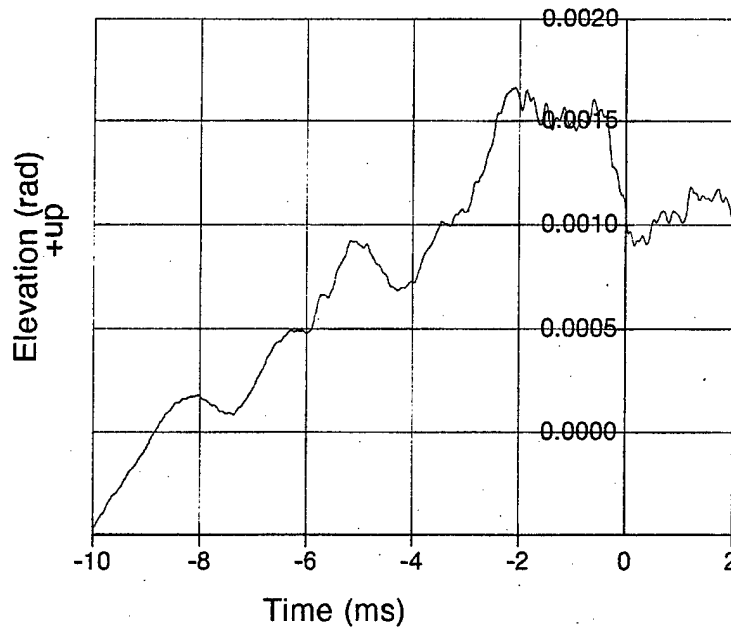


Figure 8. Vertical Component of Muzzle Pointing Angle Versus Time, Shot 34540.

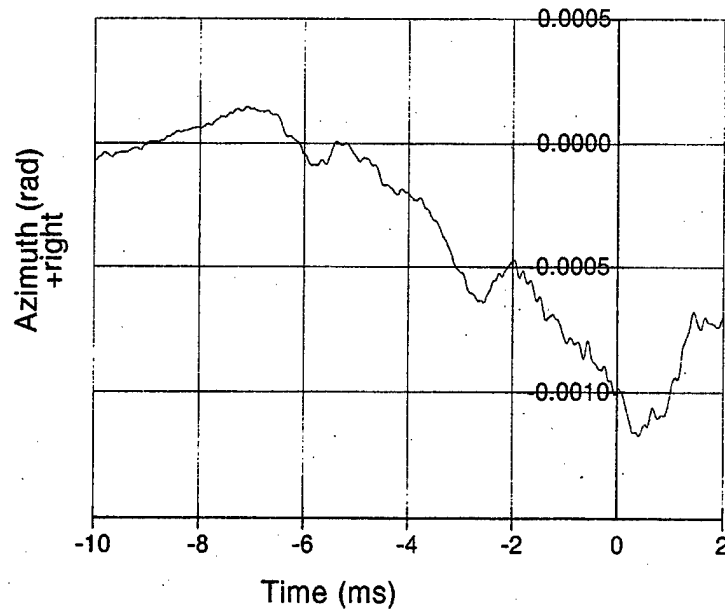


Figure 9. Horizontal Component of Muzzle Pointing Angle Versus Time, Shot 34540.

Figure 10 shows the muzzle pointing angle at shot exit for all shots with complete data. In all cases, the muzzle points up and to the gunner's left, i.e., in the second quadrant. All shots lie within a 0.5-mrad azimuth by 0.5-mrad elevation range. The horizontal and vertical SDs of dispersion are comparable even though the system demonstrates larger scale motion in the vertical plane.

Figure 11 shows the muzzle crossing velocity jump for shots with complete data. The gun lateral motion is downward for all the shots and to the left for all but one shot, i.e., almost exclusively in the third quadrant. The dispersion of the CV jump is noticeably larger than that of the PA jump. However, dispersion of the CV jump in elevation is affected by the distinct value of Shot 34546, located below the other shots in Figure 11.

4.3 Aerodynamics

The M107 projectile is a spin-stabilized, secant-ogive-cylinder-boattail configuration with physical properties and aerodynamic characteristics that have been previously reported (MacAllister & Krial 1975). In the present study, a full 6 degree-of-freedom spark range aerodynamic data reduction was performed on all 11 shots using the Aeroballistic Research Facility Data Analysis System (ARFDAS) Beta Version 4.2 software from Arrow Tech Associates, Burlington, Vermont (Hathaway & Whyte 1981). Table 5 shows results that may be useful for considering dispersion at longer ranges. The zero-yaw drag coefficient, C_{D_0} , varies from 0.318 to 0.325, approximately 2%.

The mean for all 11 shots is 0.321 and the SD is 0.0021, approximately 0.65% of the mean. Table 5 also shows the mean yaw squared, $\bar{\delta}^2$, over the 298-m range for all 11 shots and the mean value for all 11 shots, which is 0.455 deg². Two shots had values greater than 1 deg².

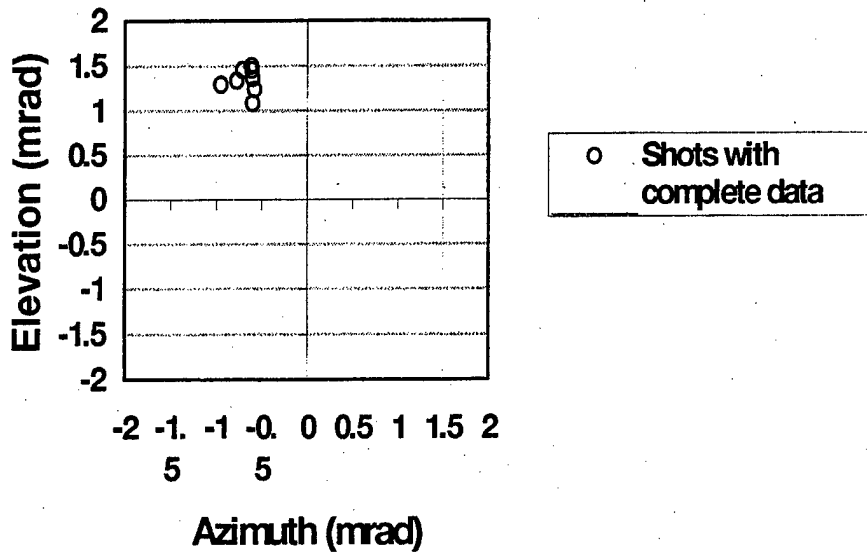


Figure 10. Muzzle Pointing Angle at Shot Exit.

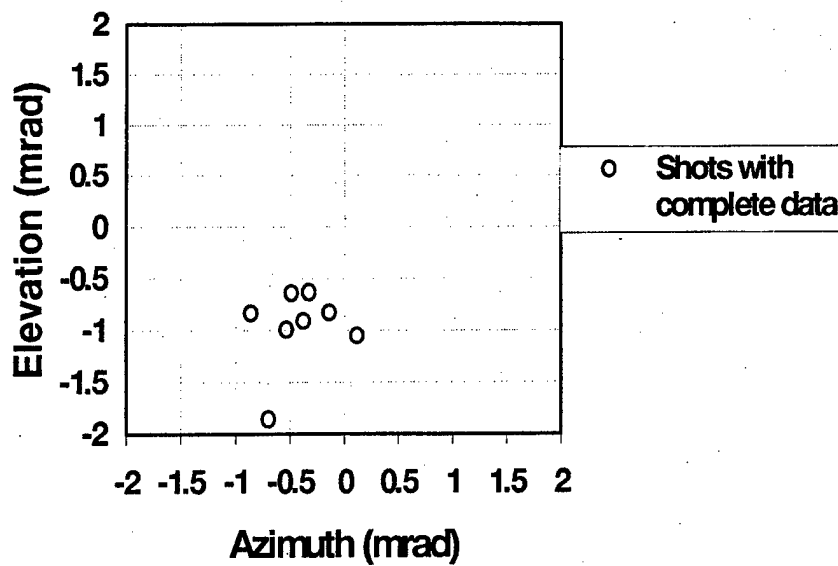


Figure 11. Muzzle Crossing Velocity (CV) Jump.

Table 5. Drag and Mean Squared Yaw

Shot	C_{D_o}	$\overline{\delta}^2$ (deg ²)	V_o (m/s)	α_o (deg)	β_o (deg)
34537	0.321	0.10	575.9	NA	NA
34538	0.318	0.03	571.4	0.09	0.01
34539	0.318	0.31	568.7	0.13	0.05
34540	0.319	0.55	573.4	0.00	0.2
34541	0.324	1.39	571.4	0.12	0.17
34542	0.320	1.08	574.1	0.00	0.00
34543	0.325	0.55	572.0	0.45	-0.10
34544	0.321	0.17	NA	NA	NA
34545	0.322	0.33	571.2	0.10	-0.05
34546	0.319	0.27	574.5	-0.02	0.10
34547	0.320	0.23	572.2	0.10	0.02
Mean	0.321	0.455			
STD	0.0021	0.423			

Table 5 also shows the measured muzzle velocity, V_o . The muzzle velocity varies from 568.7 m/s to 575.9 m/s in this group of shots, approximately 1.3% of the firing table value of 568 m/s.

The aerodynamic jump is the jump associated with aerodynamic lift forces incurred by the projectile at angle of attack. The expression for aerodynamic jump given in Equation (2) includes a contribution attributable to spin and is proportional to the initial projectile angle ξ_o . Figure 12 shows a plot of the initial projectile angle as listed in Table 5. All but one of the available shots has a measured initial total yaw with a magnitude less than 0.2° , which is on the order of the estimated accuracy of the measurement from the X-ray photographs.

The measured values of initial angle can be used in Equation (2) to calculate the spin contribution to aerodynamic jump, shown in Figure 13. The spin contribution to aerodynamic jump, denoted AJ_s , is perpendicular to the initial angle of attack. The magnitude of the spin contribution to the aerodynamic jump is calculated to be on the order of 0.1 mrad (the values are tabulated in Tables 3 and 4) for all but one shot. This level of jump is small enough to be considered within the measurement accuracy of the system. Shot 34543, however, was measured to have initial angle of attack on the order of 0.5° , producing a spin contribution to aerodynamic

jump component on the order of 0.4 mrad. Overall, however, the magnitude of the measured initial angles and spin contribution to aerodynamic jump is small enough that it is assumed to be zero for all shots and is not included in the statistical summaries of jump performance to be presented. It is noted that Shot 34543, the one shot that did have a noticeably larger value of initial yaw, impacted the target in the middle of the group. A valid observation, however, from this group of shots, is that initial yaw levels exceeding those measured in the experiment could indicate non-typical launch behavior for this system.

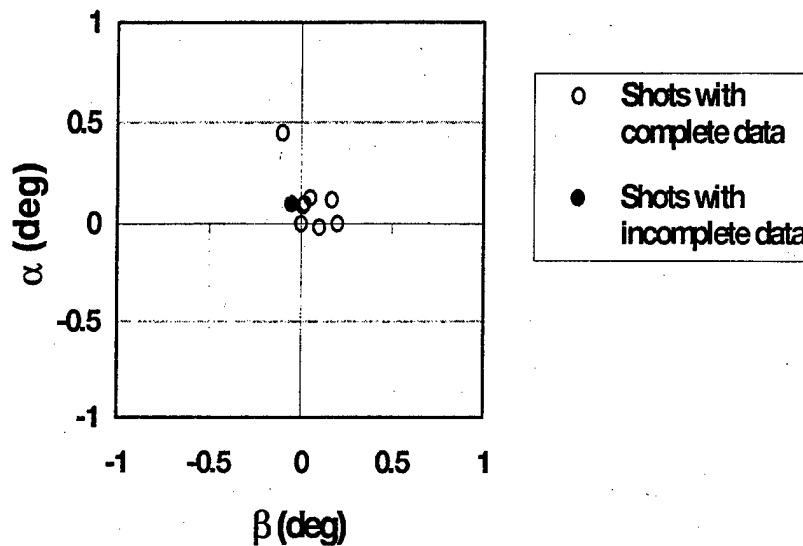


Figure 12. Initial Pitch and Yaw Angles.

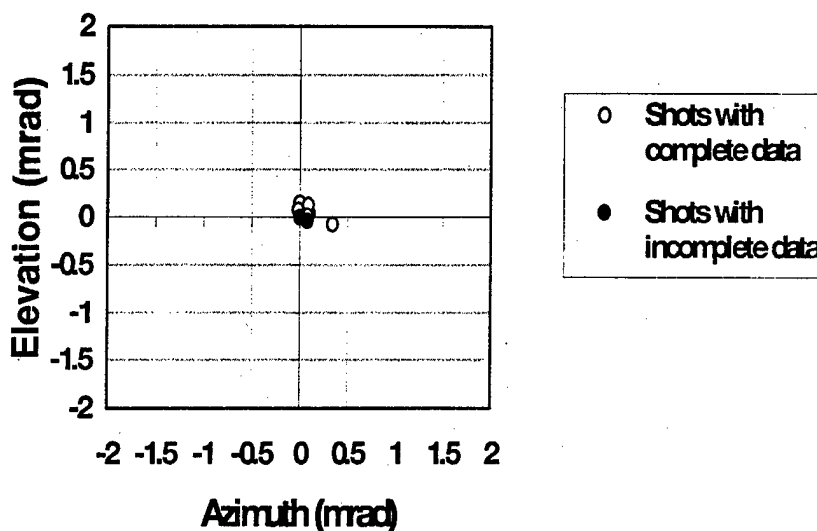


Figure 13. Spin Contribution to Aerodynamic Jump.

The non-spin component of aerodynamic is proportional to the initial transverse angular rate ξ_o^{\wedge} . Ignoring the spin contribution to aerodynamic jump, Equation (2) is used in the reduced form

$$J_A = k_t^2 (C_{L\alpha} / C_{M\alpha}) \xi_o^{\wedge} \quad \text{Eq (5)}$$

For a statically unstable (i.e., spin stabilized) spinning projectile, this component acts in the direction opposite that toward which the nose of the projectile initially rotates. (This is the opposite behavior of a statically stable non-spinning projectile such as a fin-stabilized projectile.) The components of this initial angular rate, as determined from fitting the X-ray data, are shown in Figure 14. The magnitude of the initial rate is less than approximately 1 rad/s in all cases.

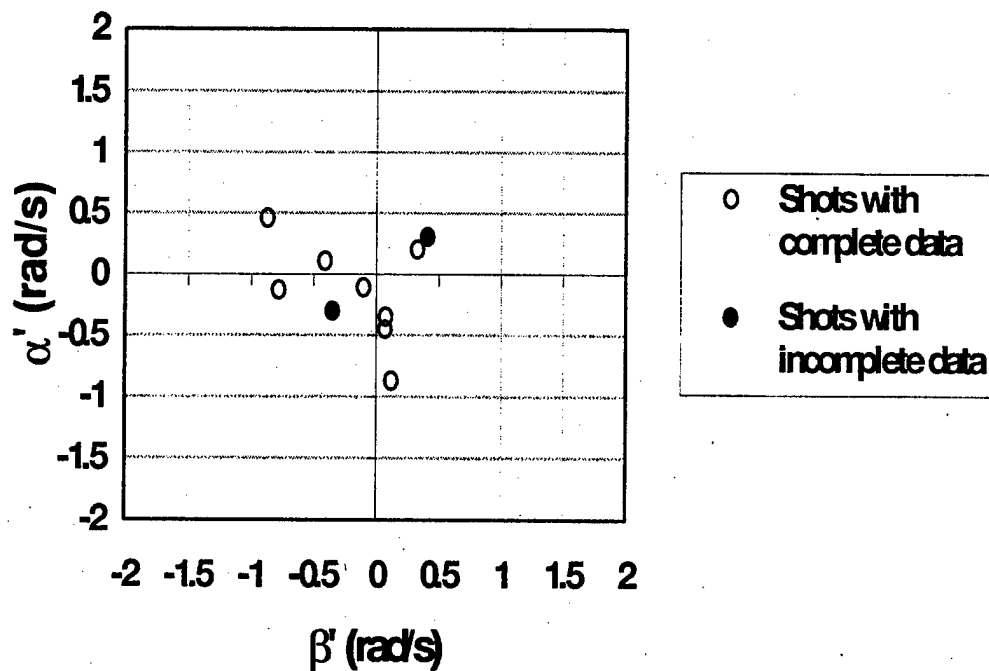


Figure 14. Initial Angular Rates in Pitch and Yaw.

These angular rates produce the aerodynamic jump results shown in Figure 15. The aerodynamic jump for each shot was calculated using a value of 0.95 for $C_{L\alpha} / C_{M\alpha}$. The magnitudes of the AJ vectors are all less than about 0.3 mrad. The mean of the AJ vectors is relatively close to zero and indicates that no noticeable bias exists. Table 3 shows that the mean of AJ is the smallest mean of any of the jump components. The SD of the dispersion of the AJ vectors is about the same in azimuth and elevation and is comparable in magnitude to that of the PA vectors. The magnitudes of the dispersions of AJ and PA are noticeably smaller than the other jump components.

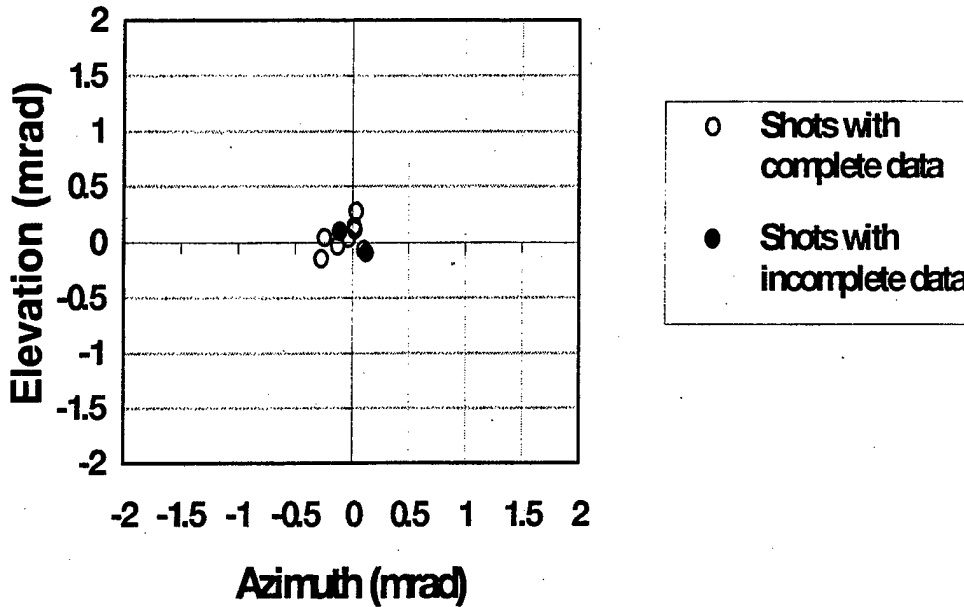


Figure 15. Aerodynamic Jump.

4.4 CG Motion at Muzzle

The projectile CG motion relative to the muzzle motion at shot exit is represented by the CG jump, shown in Figure 16. Four of the eight shots shown in the figure have CG jump magnitudes greater than 2 mrad, noticeably larger than the other jump vectors already presented. The SDs of both the horizontal and vertical CG jump components are larger than the SDs of the components of the PA, CV, and AJ jump vectors. All shots show the CG moving up and to the right relative to the bore center line motion at shot exit. The horizontal component of the CG jump appears to be larger than the vertical in both mean and dispersion, even though the gun dynamics results showed more large scale motion occurring in the vertical plane than in the horizontal plane.

The total CG jump, CG_{TOT} , was already introduced as the sum of the MP, CV, and CG jump vectors and is shown in Figure 17. This jump component demonstrates a bias up and to the right of the LOF. All the vectors of this component demonstrate upward motion; all but two of the vectors are to the right of the LOF. The magnitudes are also noticeably reduced from those of the CG jump vectors, indicating that the CG motion relative to the LOF is mitigated somewhat by the projectile interaction with the gun dynamics (MP and CV) contributions to jump.

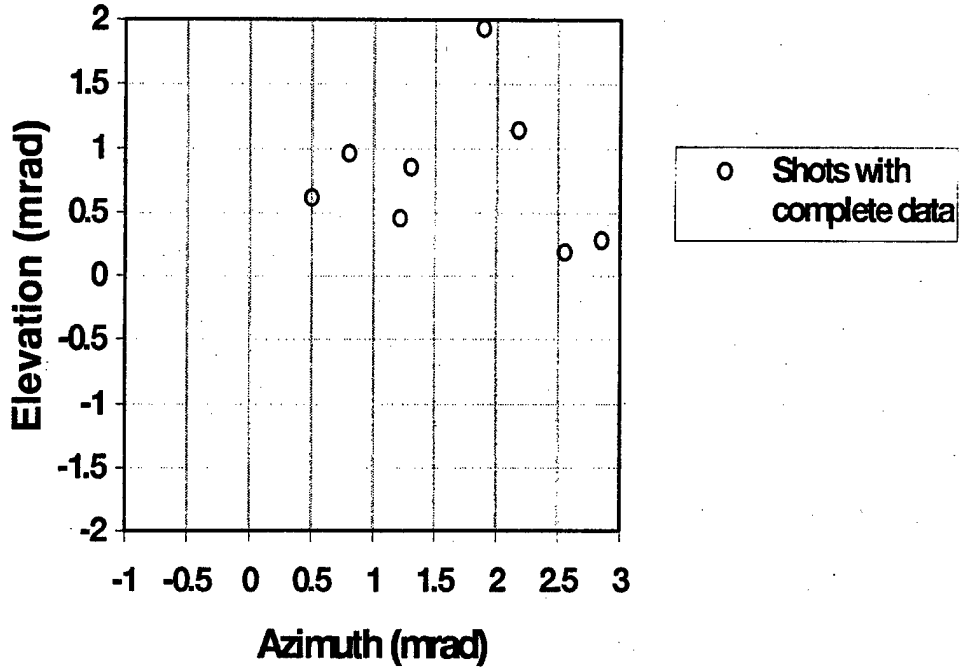


Figure 16. CG Jump.

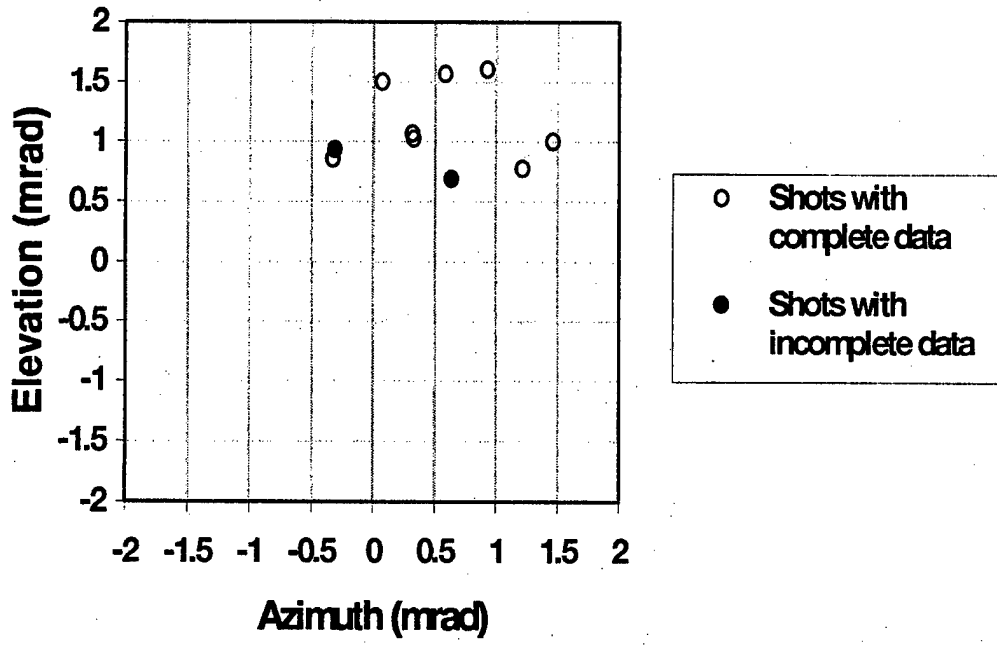


Figure 17. Total CG Jump.

4.5 Correlations Between Jump Components

A correlation coefficient was computed for each pair of jump components, total jump, and for CG_{TOT} . The correlation coefficient, denoted by r , is a statistic whose value ranges between -1 and $+1$ and indicates the degree of linear association between two sets of variables. The absolute value of r indicates the strength of the linear association. Absolute values near 1 mean that the variables are strongly correlated, so that when plotted in Cartesian coordinates, the points tend to fall along a straight line. Conversely, absolute values near 0 indicate little or no association between the variables. The sign of r indicates the direction of the linear relationship. A positive coefficient indicates that the values of the two variables increase (or decrease) together; a negative coefficient indicates that one variable increases as the other decreases. When two variables are strongly correlated, either may be usable as a predictor of the other. However, it is important to point out that a strong correlation does not imply causality. Values of r only serve as mathematical indicators of possible cause-and-effect variables; causality can only be determined after the physical relationships between the variables are carefully examined.

Table 6 is the correlation matrix for the possible pairs of total jump and jump components from Table 1, in both azimuth and elevation. Since each correlation coefficient is a statistic based upon sample data, it will in all likelihood be non-zero even for pairs of independent variables. To this extent, a hypothesis experiment was conducted upon each correlation coefficient to determine if its value was statistically significant. The hypothesis experiment yields a *P-value* associated with each correlation coefficient, listed in Table 6 as the parenthetical superscript. The range of the *P-value* is between 0 and 1. A small *P-value* of a comparison, on the order of 0.10 or less, is considered here to be statistically significant and provides confidence that the observed linear association is not attributable to inherent randomness. In Table 6, occurrences of *P-value* less than 0.01 are marked with an asterisk.

The results of Table 6 are generated from the jump components as depicted graphically in component matrix plots. The matrix plots for the components in azimuth and elevation are shown in Figures 18 and 19, respectively. The matrix plot consists of subplots of each pair of jump components on the appropriate off-diagonal element of the matrix. The scale of each subplot is linear and spans the range of values for the respective jump component. Each subplot shows the plotted value of the individual jump component for each shot, as labeled using the final two digits of the shot number.

The fitted linear regression is graphically included in each subplot. A qualitative indicator of the strength of the linear correlation between two jump components is the closeness of

individual points to the line that represents the linear regression. The matrix plots also include histograms for each jump component on the diagonal showing the distribution of each component across its range of values.

Table 6. Correlation Matrices for Total Jump and All Jump Components

Azimuth					
	MP	CV	CG	AJ	Total
MP	1.000 (N/A)				
CV	0.596 (0.069*)	1.000 (N/A)			
CG	-0.589 (0.073*)	-0.962 (<0.001*)	1.000 (N/A)		
AJ	0.460 (0.181)	0.262 (0.464)	-0.423 (0.224)	1.000 (N/A)	
Total	0.146 (0.687)	-0.623 (0.054*)	0.700 (0.024*)	-0.069 (0.849)	1.000 (N/A)
Elevation					
	MP	CV	CG	AJ	Total
MP	1.000 (N/A)				
CV	0.021 (0.954)	1.000 (N/A)			
CG	-0.162 (0.655)	-0.916 (<0.001*)	1.000 (N/A)		
AJ	-0.020 (0.955)	0.154 (0.671)	-0.113 (0.757)	1.000 (N/A)	
Total	0.591 (0.072*)	-0.155 (0.668)	0.324 (0.362)	0.354 (0.315)	1.000 (N/A)

Table 6 shows that, in elevation, only one comparison of jump components, CV versus CG, has a correlation coefficient whose magnitude approaches 1 with a statistically significant *P-value*. With a value of $r = -0.916$, this pair of jump components exhibits a strong negative correlation in elevation. This same pair of jump components exhibits a similar strong, statistically significant, negative correlation in azimuth, with a value of $r = -0.962$. The correlation demonstrates that the two components consistently act in opposite directions. One physical interpretation is that the muzzle crossing velocity at shot exit is dominated by motion with a large enough frequency (possibly a vibrational perturbation) to which the projectile CG does not respond before disengaging from the gun tube.

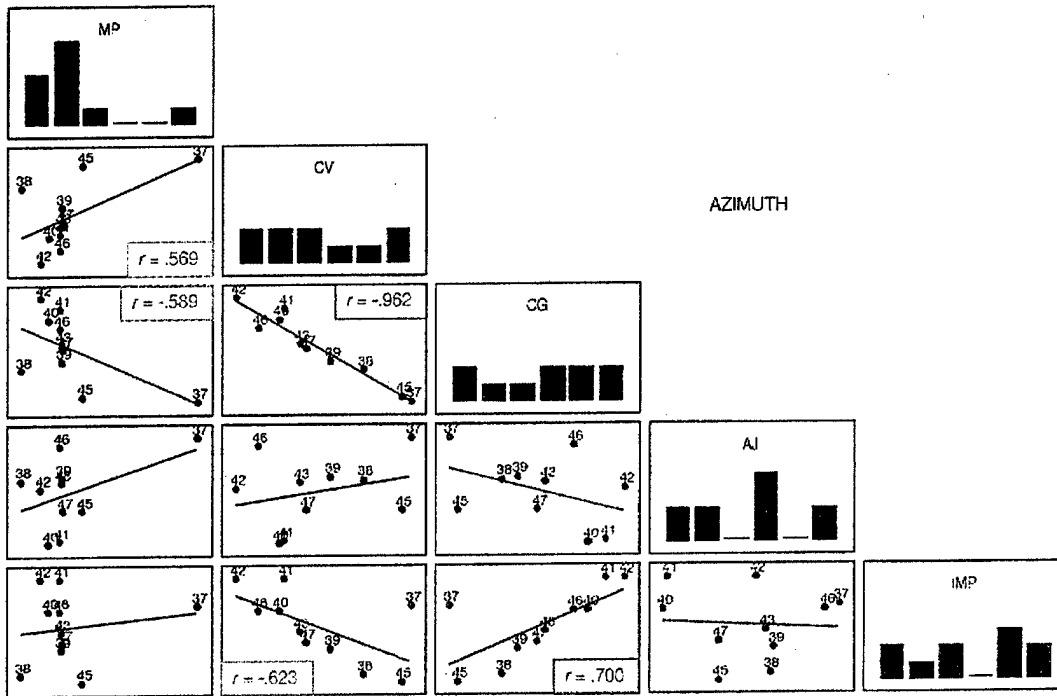


Figure 18. Matrix Plot for Total Jump and All Jump Components, Azimuth.

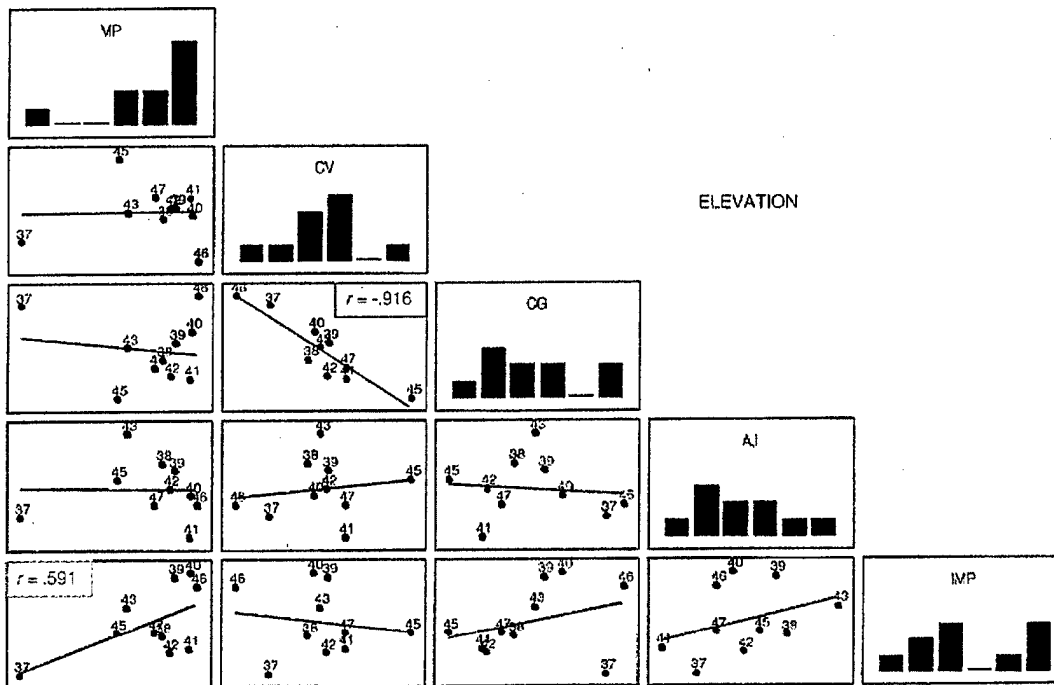


Figure 19. Matrix Plot for Total Jump and All Jump Components, Elevation.

Only one other comparison of jump components in elevation, muzzle pointing angle (MP) versus total jump (denoted in the matrix plot as IMP), has a statistically significant *P-value*. However, the statistical significance of the correlation is maintained only by the presence of an outlier, Shot 34537, as indicated by the MP histogram. When the shot is removed from the comparison between MP and IMP, statistical significance is lost. Furthermore, the comparison of these two quantities in azimuth, either with or without Shot 34537, does not yield a correlation coefficient that is statistically significant. This is unlike the previously mentioned correlation between CV and CG, in which the statistical significance of the correlation (1) existed in both azimuth and elevation and (2) did not depend on the inclusion of any particular shot. It is concluded that no statistically significant correlation exists between the muzzle pointing angle and the total jump for this group of shots.

In azimuth, the MP jump shows statistically significant correlation coefficients to exist when compared to either CV jump or CG jump. However, as in the case of MP versus IMP in elevation, as discussed in the previous paragraph, the significance of the correlation is maintained only by the presence of the outlier, Shot 34537. Following the same reasoning, it is concluded that no statistically significant correlation exists in the comparisons of MP versus CV and MP versus CG.

Two other statistically significant correlation coefficients exist in azimuth: CV versus IMP, with $r = -0.623$, and CG versus IMP, with $r = 0.700$. In both cases, Shot 34537 does not maintain the statistical significance of the correlation coefficients, and its removal only strengthens the correlation in the comparisons.

Table 7 shows the matrices of correlation coefficients between the total jump, CG_{TOT} , and AJ jump. Figures 20 and 21 show the corresponding matrix plots and histograms. Statistically significant correlation coefficients exist in the comparisons between CG_{TOT} and the total jump in both azimuth and elevation. The correlation shows that the trajectory of the projectile CG at shot exit relative to the LOF primarily determines the total jump of the shot. The aerodynamic jump, on the other hand, has a minimal effect, with no significant correlation with the total jump and magnitudes of mean and dispersion that are small, as discussed earlier.

A graphical procedure for exhibiting the most important jump component correlations is shown in Figure 22 and is based upon the mathematical equation:

$$\sigma_{IMPACT}^2 = \sigma_{MP}^2 + \sigma_{CV}^2 + \sigma_{CG}^2 + \sigma_{AJ}^2 + 2[Cov(MP, CV) + \dots + Cov(CG, AJ)]$$

Table 7. Correlation Matrices for Total Jump, CG_{TOT}, and AJ Jump Components

Azimuth			
	CG _{TOT}	AJ	Total
CG	1.000 (N/A)		
AJ	-0.284 (0.426)	1.000 (N/A)	
Total	0.976(<0.001*)	-0.069 (0.849)	1.000 (N/A)
Elevation			
	CG _{TOT}	AJ	Total
CG	1.000 (N/A)		
AJ	-0.001 (0.999)	1.000 (N/A)	
Total	0.935(<0.001*)	0.354 (0.315)	1.000 (N/A)

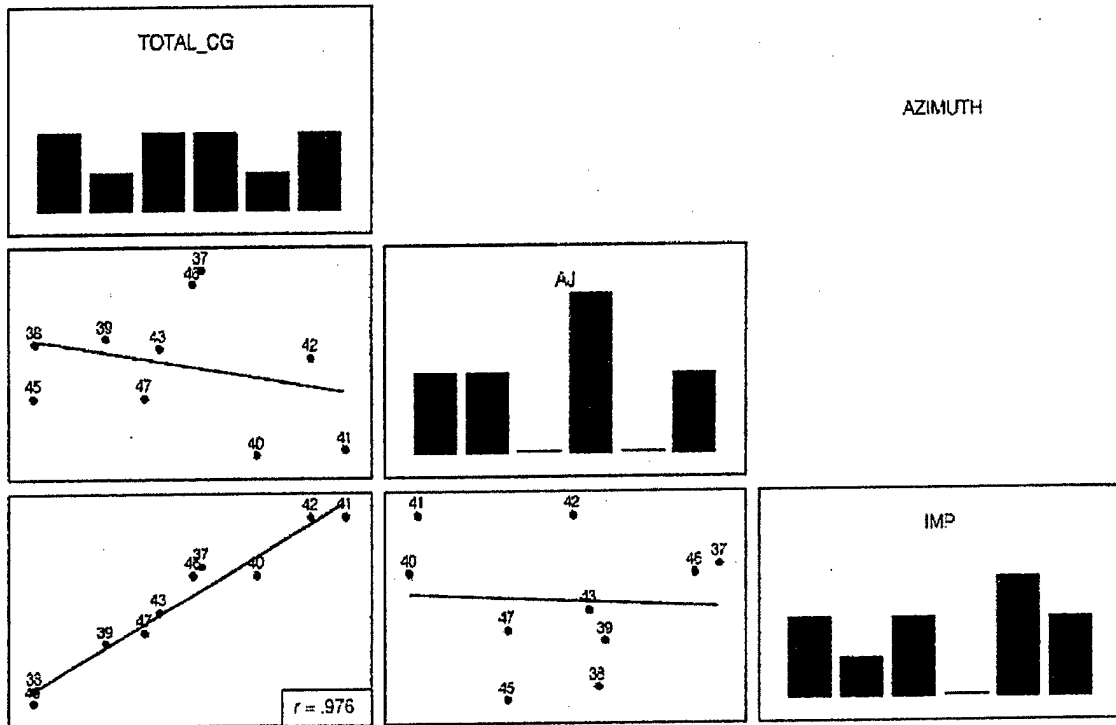


Figure 20. Matrix Plot for Total Jump, CG_{TOT}, and AJ Jump Components, Azimuth.

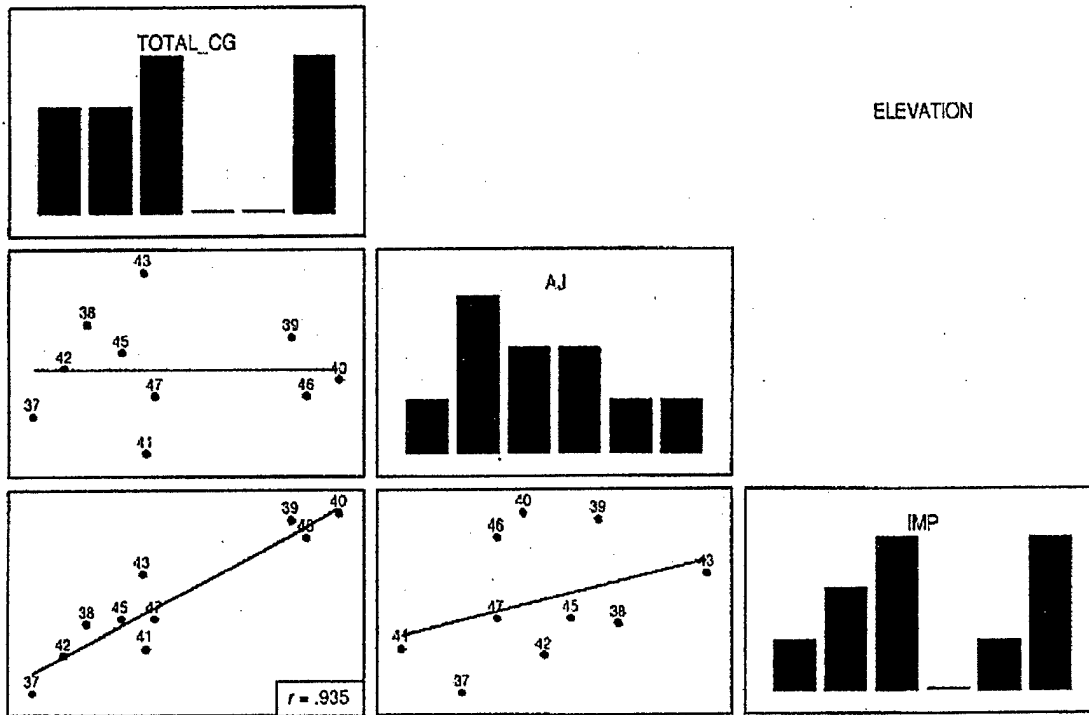


Figure 21. Matrix Plot for Total Jump, CGTOT, and AJ Jump Components, Elevation.

in which for example, $Cov(MP, CV) = \rho_{MP, CV} \sigma_{MP} \sigma_{CV}$. This formula relates σ_{IMPACT}^2 with the variations of the individual jump components. The root sum square (RSS) of the variance components, $\sqrt{\sigma_{MP}^2 + \sigma_{CV}^2 + \sigma_{CG}^2 + \sigma_{AJ}^2}$, overestimates the dispersion of the impacts, σ_{IMPACT} . By adding the largest covariances to the RSS, we “close the loop” so to speak, and bring this quantity nearer to σ_{IMPACT} . The addition of $Cov(CV, CG)$ to the RSS brings the most closure to the model, while adding the covariances of the other in-bore jump components brings the RSS and σ_{IMPACT} nearer still.

5. CONCLUSION

A jump experiment and analysis were performed for the M198 howitzer firing the M107 projectile through a short range, flat fire trajectory with a launch Mach number near 1.7. The objective was to characterize the jump performance of the system and provide a basis for identifying and possibly improving the largest contributors to jump over a broader range of firing conditions.

For the short range, flat fire scenario of the present experiment, the jump performance of the system indicates that aerodynamic jump is a significantly smaller contributor to the jump means and dispersions than the projectile CG motion at shot exit. The CG jump demonstrated the largest

dispersion of any of the measured jump components, suggesting the presence of significant in-bore balloting relative to the muzzle itself. The dispersion of the total CG jump, CG_{TOT} was only about half that of the CG jump alone but was still large compared to the dispersion of the other jump components.

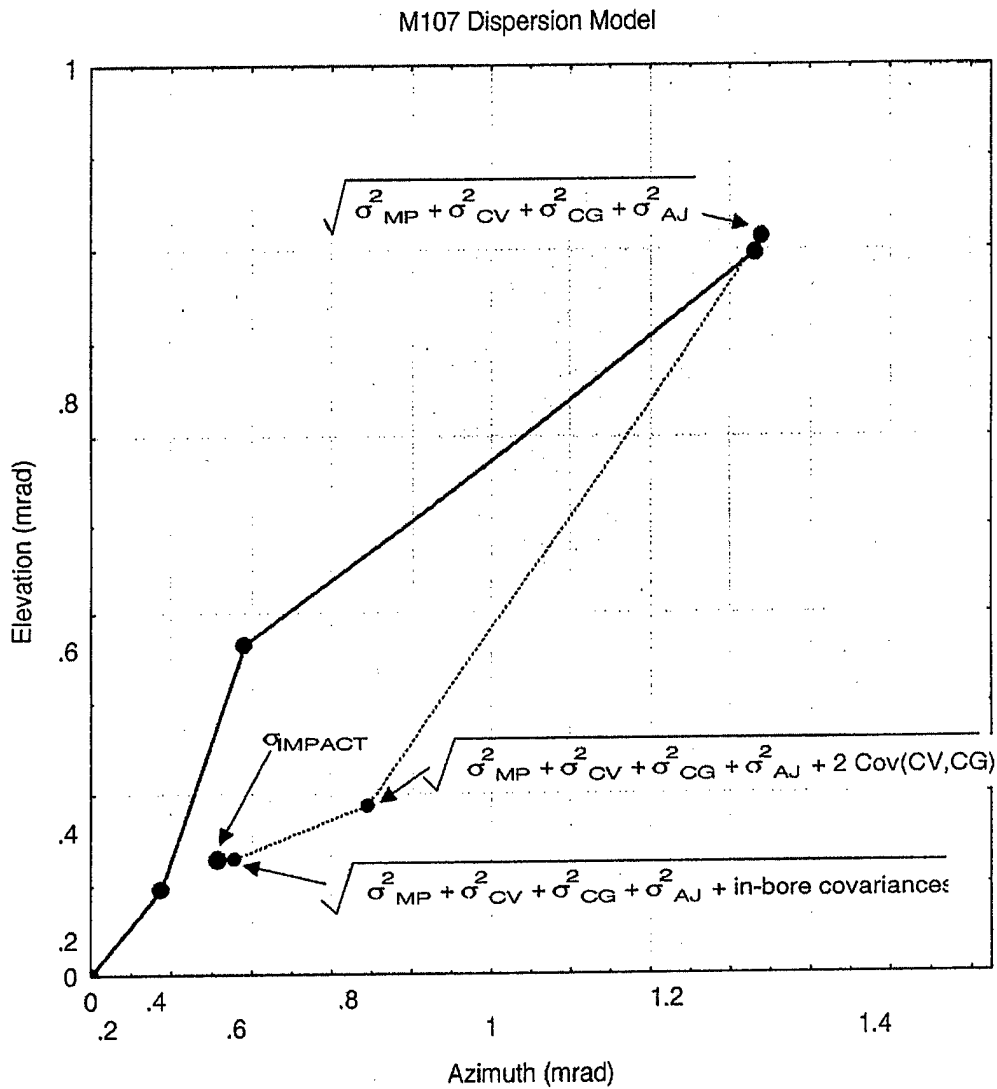


Figure 22. M107 Jump Closure.

The aerodynamic jump was small because of the low levels of initial projectile yaw and yaw rate. Overall, the group demonstrated small yaw levels. All initial angular rates were about 1 rad/s or less in magnitude. All initial angles were less than 0.2° in magnitude except for one shot that had a magnitude of about 0.4° . The initial yaw levels approached the measurement accuracy of the system and produced spin contributions to aerodynamic jump that were

considered too small to include in the present jump model. It is noted that initial angles on the order of 1° could be considered abnormal by comparison and would contribute more significantly to the spin contribution to aerodynamic jump.

For all shots, the muzzle was pointed up and to the left at shot exit, and the muzzle crossing velocity was down and to the left for all but one shot. The large scale muzzle motion was more pronounced in the vertical plane than in the horizontal plane. This motion dominates the mean values of the PA and CV jump vectors, but the dispersion in PA and CV is about the same in azimuth and elevation. Even though more vertical gun tube motion is evident than horizontal motion, the dispersion of the CG and CG_{TOT} jump vectors is larger in azimuth than elevation.

The variability in the projectile initial lateral CG motion appears to be a more important effect than the projectile initial angular motion for the short range, flat fire scenario. This observation may be useful for efforts focused on enhancing artillery accuracy at longer ranges. Additionally, the measurements of muzzle velocity, drag, and yaw may be useful for determining the effect of jump components not directly measured here but important for longer ranges. This experiment represents an initial effort that will contribute to a unified database characterizing the weapon system performance over a wider range of firing conditions.

The results from the jump experiment apply to both the precision and accuracy models for artillery. The present accuracy model is composed of several terms, including meteorological effects and inaccuracies in their measurement, muzzle velocity variations, quadrant elevation deviations, ballistic coefficient deviations and weapon location inaccuracies as given by Reichelderfer (1993):

$$\sigma_R^2 = \frac{\partial R^2}{\partial W} (\sigma_w^2) + \frac{\partial R^2}{\partial T} (\sigma_T^2) + \frac{\partial R^2}{\partial D} (\sigma_D^2 + \sigma_{o-o}^2) + \frac{\partial R^2}{\partial V} (\sigma_V^2) + \frac{\partial R^2}{\partial QE} (\sigma_A^2 + \sigma_{WL}^2)$$

The results from this experiment are applicable to describing the errors in quadrant elevation and to some extent, the ballistic coefficient deviations. The quadrant elevation angle range error can be improved by incorporating an average vertical jump term. The total jump vector is by definition the sum of the PA, CV, CG, and AJ vertical components for artillery. This quantity is the combination of the gun effects on the projectile. This component added to the quadrant angle can be used to refine the quadrant angle error term.

$$\left(\frac{\partial R^2}{\partial QE} \sigma_A^2 \right).$$

The artillery precision model that describes dispersion about a mean point of impact is somewhat simpler and contains three groups of terms. These are classed as muzzle velocity errors, quadrant elevation errors, and ballistic coefficient errors.

$$PE^2_R = (PE_{mv} \frac{\Delta R}{\Delta mv})^2 + (PE_{QE} \frac{\Delta R}{\Delta QE})^2 + (PE_C \frac{\Delta R}{\Delta C})^2$$

The jump vectors are again relevant to the components of the precision model. The quadrant elevation errors

$$(PE_{QE} \frac{\Delta R}{\Delta QE})^2$$

are proportional to SDs in total jump vector. Precision probable errors in ballistic coefficient also seem to be insensitive to quadrant elevation changes from 0° to 45° as the same value is used (Kogler 1995). As flight times for long range projectile versions increase, drag errors affect the trajectory more substantially. The source of these drag errors is a complex combination of yaw drag, yaw of repose, and projectile limit cycle yaw. Accurately allocating errors to meteorological, mechanical, or aerodynamic sources is an important step in minimizing system errors.

REFERENCES

- Bornstein, J., I. Celmins, and P. Plostins, "Launch Dynamics of Fin-Stabilized Projectiles," AIAA Paper No. 89-3395, August 1989.
- Bornstein, J., I. Celmins, P. Plostins, and E.M. Schmidt, "Techniques for the Measurement of Tank Cannon Jump," BRL-MR-3715, U.S. Army Ballistic Research Laboratory, Aberdeen Proving Ground, Maryland, December 1988.
- Bornstein, J., and B. Haug, "Gun Dynamics Measurements for Tank Gun Systems," BRL-MR-3688, U.S. Army Ballistic Research Laboratory, Aberdeen Proving Ground, Maryland, May 1988.
- Hathaway, W., and R. Whyte, "Free Flight Range Data Reduction," ARFDAS User Manual, Armament and Electrical Systems Department, General Electric Company, Burlington, VT, 1981.
- Headquarters, Department of the Army, Firing Table (FT) 155-AM-2, Washington, DC, March 1983.
- Kogler, T., "The 155-mm Ultra-Lightweight Field Howitzer: Indirect Fire Precision," U.S. Army Research Laboratory Report ARL-MR-265, Aberdeen Proving Ground, Maryland, July 1995.
- Lyon, D.H., D.S. Savick, and E.M. Schmidt, "Comparison of Computed and Measured Jump of 120-mm Cannon," AIAA Paper 91-2898, July 1991.
- MacAllister, L.C., and K.S. Krial, "Aerodynamic Properties and Stability Behavior of the 155-mm Howitzer Shell, M107," BRL-MR-2547, U.S. Army Ballistic Research Laboratory, Aberdeen Proving Ground, Maryland, October 1975.
- McCoy, R.L., "Modern Exterior Ballistics," Schiffer Publishing Ltd, Atglen, PA, 1998.
- Murphy, C.H., "Free Flight Motion of Symmetric Missiles," Report No. 1216, Ballistic Research Laboratories, Aberdeen Proving Ground, Maryland, July 1963.
- Plostins, P., "Launch Dynamics of APFSDS Ammunition," BRL-TR-2595, U.S. Army Ballistic Research Laboratory, Aberdeen Proving Ground, Maryland, October 1984.
- Plostins, P., I. Celmins, and J. Bornstein, "The Effect of Sabot Front Borerider Stiffness on the Launch Dynamics of Fin-Stabilized Kinetic Energy Ammunition," AIAA Paper No. 90-0066, January 1990.

Reichelderfer, M. "155-mm Howitzer Accuracy and Effectiveness Analysis," Division Note (DN)-G-32, U.S. Army Materiel Systems Analysis Activity, Aberdeen Proving Ground, Maryland, 1993.

Rogers, W., "The Transonic Free Flight Range," Report No. 849, U.S. Army Research Laboratory, Aberdeen Proving Ground, Maryland, September 1969.

APPENDIX A
M107 JUMP STATISTICAL REVIEW

INTENTIONALLY LEFT BLANK

M107 JUMP STATISTICAL REVIEW

Means of Jump and Components 155-mm M107

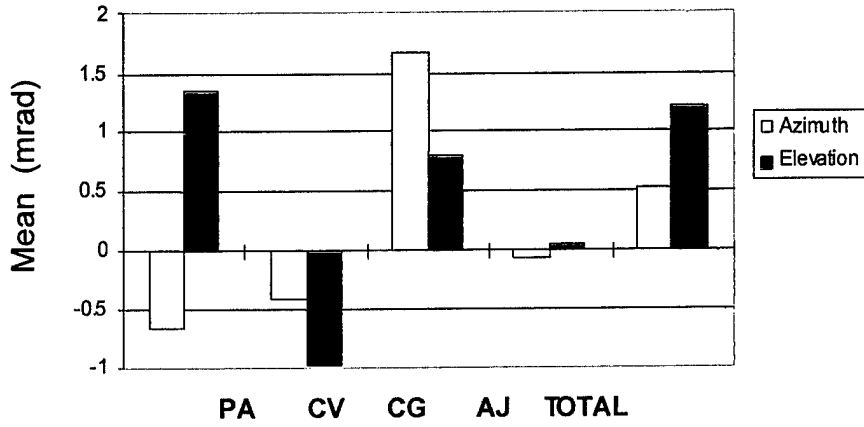


Figure A-1. Means of Jump and Jump Components.

Dispersions of Jump and Components 155-mm M107

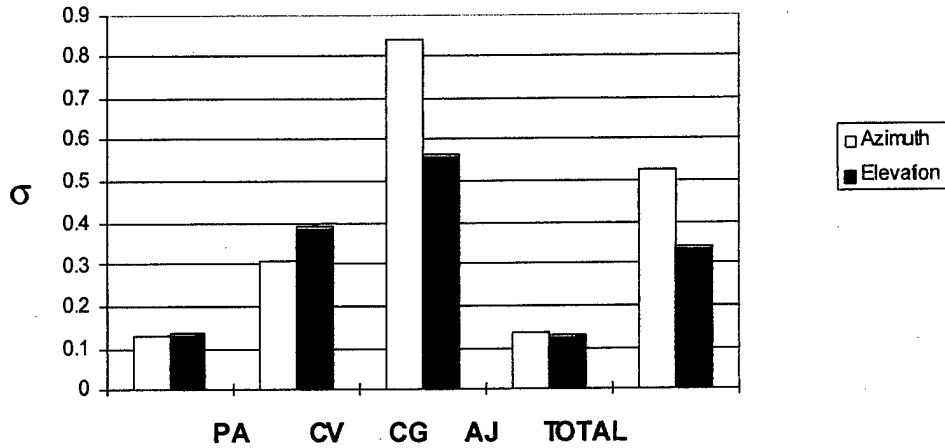


Figure A-2. Standard Deviations of Dispersions of Jump and Jump Components.

**Means of Other Jump Components
155-mm M107**

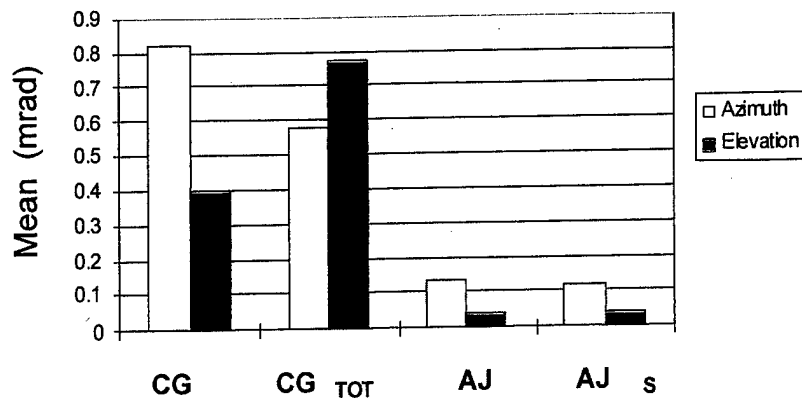


Figure A-3. Means of Other Jump Components.

**Dispersion of Other Jump Components
155-mm M107**

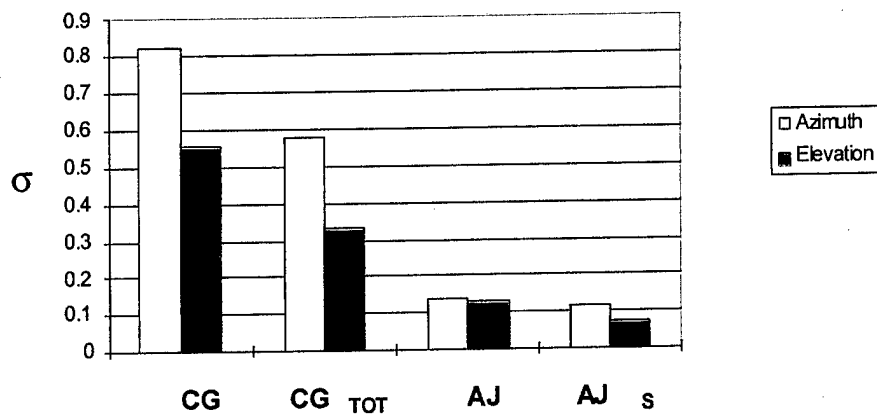


Figure A-4. Standard Deviations of Dispersions of Other Jump Components.

APPENDIX B
LIST OF SYMBOLS

INTENTIONALLY LEFT BLANK

LIST OF SYMBOLS

d	reference diameter
$C_{L\alpha}$	lift force coefficient
$C_{M\alpha}$	pitching moment coefficient
J_A	aerodynamic jump (jump attributable to aerodynamic lift)
k_t	transverse gyroscopic radius
R	range
s	distance along flight path in calibers
t	time
X, Y	jump coordinates
Re	real part of complex number
Im	imaginary part of complex number

Greek Symbols

α	pitch angle, positive nose up
β	yaw angle, positive nose left looking downrange
δ	total yaw, $(\alpha^2 + \beta^2)^{1/2}$
ξ	complex yaw angle, $\beta + i\alpha$
σ	one standard deviation
θ	total jump vector
θ_h	horizontal component of total jump
θ_v	vertical component of total jump

Subscripts

H	horizontal component
V	vertical component
0	initial condition
T	evaluated at target location

Superscripts

$(\)$	derivative with respect to s
--------	--------------------------------

INTENTIONALLY LEFT BLANK

<u>NO. OF COPIES</u>	<u>ORGANIZATION</u>	<u>NO. OF COPIES</u>	<u>ORGANIZATION</u>
2	ADMINISTRATOR DEFENSE TECHNICAL INFO CENTER ATTN DTIC OCP 8725 JOHN J KINGMAN RD STE 0944 FT BELVOIR VA 22060-6218	1	US ARMY NATICK RDEC ACTING TECHNICAL DIR ATTN SSCNC T P BRANDLER NATICK MA 01760-5002
1	DIRECTOR US ARMY RESEARCH LABORATORY ATTN AMSRL CS AS REC MGMT 2800 POWDER MILL RD ADELPHI MD 20783-1197	1	US ARMY SIMULATION TRAIN & INSTRMNTN CMD ATTN J STAHL 12350 RESEARCH PARKWAY ORLANDO FL 32826-3726
1	DIRECTOR US ARMY RESEARCH LABORATORY ATTN AMSRL CI LL TECH LIB 2800 POWDER MILL RD ADELPHI MD 207830-1197	1	US ARMY TANK-AUTOMOTIVE & ARMAMENTS CMD ATTN AMSTA AR TD M FISETTE BLDG 1 PICATINNY ARSENAL NJ 07806-5000
1	DIRECTOR US ARMY RESEARCH LABORATORY ATTN AMSRL DD J J ROCCHIO 2800 POWDER MILL RD ADELPHI MD 20783-1197	1	US ARMY TRAINING & DOCTRINE CMD BATTLE LAB INTEGRATION & TECH DIR ATTN ATCD B J A KLEVECZ FT MONROE VA 23651-5850
1	DOD JOINT CHIEFS OF STAFF ATTN J39 CAPABILITIES DIV CAPT J M BROWNELL THE PENTAGON RM 2C865 WASHINGTON DC 20301	1	NAV SURFACE WARFARE CTR ATTN CODE B07 J PENNELLA 17320 DAHLGREN RD BLDG 1470 RM 1101 DAHLGREN VA 22448-5100
1	OSD ATTN OUSD(A&T)/ODDDR&E(R) ATTN R J TREW THE PENTAGON WASHINGTON DC 20310-0460	1	DARPA ATTN B KASPAR 3701 N FAIRFAX DR ARLINGTON VA 22203-1714
1	AMCOM MRDEC ATTN AMSMI RD W C MCCORKLE REDSTONE ARSENAL AL 35898-5240	1	UNIV OF TEXAS HICKS & ASSOCIATES, INC. ATTN G SINGLEY III 1710 GOODRICH DR STE 1300 MCLEAN VA 22102
1	CECOM ATTN PM GPS COL S YOUNG FT MONMOUTH NJ 07703	1	HQ AFWA/DNX 106 PEACEKEEPER DR STE 2N3 OFFUTT AFB NE 68113-4039
1	CECOM SP & TERRESTRIAL COMMCTN DIV ATTN AMSEL RD ST MC M H SOICHER FT MONMOUTH NJ 07703-5203		<u>ABERDEEN PROVING GROUND</u>
1	US ARMY INFO SYS ENGRG CMD ATTN ASQB OTD F JENIA FT HUACHUCA AZ 85613-5300	2	DIRECTOR US ARMY RESEARCH LABORATORY ATTN AMSRL CI LP (TECH LIB) BLDG 305 APG AA
		1	CDR USATECOM AMSTE TE F L TELETSKI RYAN BLDG

NO. OF
COPIES ORGANIZATION

1 COMMANDER
 US ARMY ABERDEEN TEST CENTER
 STEC LI
 BLDG 400

5 CDR US ARMY TACOM ARDEC
 ATTN AMSTA AR FSF T
 R LIESKE J MATTS
 F MIRABELLE R PUHALLA
 J WHITESIDE
 BLDG 120

1 DIRECTOR
 US ARMY MATERIEL SYSTEMS
 ANALYSIS ACTIVITY
 ATTN AMXSY CA R NORMAN
 BLDG 367

1 DIR USARL
 ATTN AMSRL WM B A W HORST JR
 BLDG 4600

3 DIR USARL
 ATTN AMSRL WM BA W D'AMICO
 F BRANDON L BURKE
 BLDG 4600

21 DIR USARL
 ATTN AMSRL WM BC P PLOSTINS
 H EDGE T ERLINE
 J GARNER (5 CYS) B GUIDOS
 D LYON A MIKHAIL
 J NEWILL V OSKAY
 B PATTON C RUTH
 J SAHU K SOENCKSEN
 D WEBB P WEINACHT
 S WILKERSON A ZIELINSKI
 BLDG 390

ABSTRACT ONLY

1 DIRECTOR
 US ARMY RESEARCH LABORATORY
 ATTN AMSRL CS EA TP TECH PUB BR
 2800 POWDER MILL RD
 ADELPHI MD 20783-1197

REPORT DOCUMENTATION PAGE

Form Approved
OMB No. 0704-0188

Public reporting burden for this collection of information is estimated to average 1 hour per response, including the time for reviewing instructions, searching existing data sources, gathering and maintaining the data needed, and completing and reviewing the collection of information. Send comments regarding this burden estimate or any other aspect of this collection of information, including suggestions for reducing this burden, to Washington Headquarters Services, Directorate for Information Operations and Reports, 1215 Jefferson Davis Highway, Suite 1204, Arlington, VA 22202-4302, and to the Office of Management and Budget, Paperwork Reduction Project (0704-0188), Washington, DC 20503.

1. AGENCY USE ONLY (Leave blank)		2. REPORT DATE September 1999		3. REPORT TYPE AND DATES COVERED Final	
4. TITLE AND SUBTITLE Flat Fire Jump Performance of a 155-mm M198 Howitzer				5. FUNDING NUMBERS Project No. 1L1622618.AH80	
6. AUTHOR(S) Garner, J.M.; Guidos, B.J.; Soencksen, K.P.; Webb, D.W. (all of ARL)					
7. PERFORMING ORGANIZATION NAME(S) AND ADDRESS(ES) U.S. Army Research Laboratory Weapons & Materials Research Directorate Aberdeen Proving Ground, MD 21010-5066				8. PERFORMING ORGANIZATION REPORT NUMBER	
9. SPONSORING/MONITORING AGENCY NAME(S) AND ADDRESS(ES) U.S. Army Research Laboratory Weapons & Materials Research Directorate Aberdeen Proving Ground, MD 21010-5066				10. SPONSORING/MONITORING AGENCY REPORT NUMBER ARL-TR-2067	
11. SUPPLEMENTARY NOTES					
12a. DISTRIBUTION/AVAILABILITY STATEMENT Approved for public release; distribution is unlimited.				12b. DISTRIBUTION CODE	
13. ABSTRACT (Maximum 200 words) A jump experiment and analysis were performed for the M198 howitzer firing the M107 shell through short range, flat fire trajectories with a launch Mach number near 1.7. The objective was to characterize the jump performance of the system and provide a basis for identifying and possibly improving the largest contributors to jump over a broader range of firing conditions. For the short range, flat fire scenario of the present experiment, the jump performance of the system indicates that the center of gravity (CG) motion of the projectile as it exits the gun tube is a significantly larger contributor to dispersion than the aerodynamic jump. The data showed that the projectile CG motion relative to the muzzle itself is considerable and is a more dominant component of in-bore balloting in terms of dispersion compared to the in-bore angular motion. Measurements of the gun dynamics showed that while the large scale muzzle motion is more pronounced in the vertical plane than in the horizontal plane, the dispersion directly attributable to muzzle pointing angle and muzzle crossing velocity is about the same in the both directions. Measurements of muzzle velocity, drag, and yaw are also presented and can be used to determine the effect of jump components not directly measured here but important for longer ranges.					
14. SUBJECT TERMS aerodynamic jump artillery				15. NUMBER OF PAGES 50	
				16. PRICE CODE	
17. SECURITY CLASSIFICATION OF REPORT Unclassified		18. SECURITY CLASSIFICATION OF THIS PAGE Unclassified		19. SECURITY CLASSIFICATION OF ABSTRACT Unclassified	
20. LIMITATION OF ABSTRACT					